ARTICLE

doi:10.1038/nature13240

Space–time wiring specificity supports direction selectivity in the retina

Jinseop S. Kim[1]*, Matthew J. Greene[1]*, Aleksandar Zlateski[2], Kisuk Lee[1], Mark Richardson[1]†, Srinivas C. Turaga[1]†, Michael Purcaro[1], Matthew Balkam[1], Amy Robinson[1], Bardia F. Behabadi[3], Michael Campos[3], Winfried Denk[4], H. Sebastian Seung[1]† & the EyeWirers[5]

How does the mammalian retina detect motion? This classic problem in visual neuroscience has remained unsolved for 50 years. In search of clues, here we reconstruct Off-type starburst amacrine cells (SACs) and bipolar cells (BCs) in serial electron microscopic images with help from EyeWire, an online community of 'citizen neuroscientists'. On the basis of quantitative analyses of contact area and branch depth in the retina, we find evidence that one BC type prefers to wire with a SAC dendrite near the SAC soma, whereas another BC type prefers to wire far from the soma. The near type is known to lag the far type in time of visual response. A mathematical model shows how such 'space–time wiring specificity' could endow SAC dendrites with receptive fields that are oriented in space–time and therefore respond selectively to stimuli that move in the outward direction from the soma.

Compared to cognitive functions such as language, the visual detection of motion may seem trivial, yet the underlying neural mechanisms have remained elusive for half a century[1,2]. Some retinal outputs (ganglion cells) respond selectively to visual stimuli moving in particular directions, whereas retinal inputs (photoreceptors) lack direction selectivity (DS). How does DS emerge from the microcircuitry connecting inputs to outputs?

Research on this question has converged upon the SAC (Fig. 1a, b). A SAC dendrite is more strongly activated by motion outward from the cell body to the tip of the dendrite, than by motion in the opposite direction[3]. Therefore a SAC dendrite exhibits DS, and outward motion is said to be its 'preferred direction'. Note that it is incorrect to assign a single such direction to a SAC, because each of the cell's dendrites has its own preferred direction (Fig. 1a). DS persists after blocking inhibitory synaptic transmission[4], when the only remaining inputs to SACs are BCs, which are excitatory. As the SAC exhibits DS but its BC inputs exhibit little or none[5], DS appears to emerge from the BC–SAC circuit.

Mouse BCs have been classified into multiple types[6], with different time lags in visual response[7,8]. Motion is a spatiotemporal phenomenon: an object at one location appears somewhere else after a time delay. Accordingly, DS might arise because different locations on the SAC dendrite are wired to BC types with different time lags. More specifically, we propose that the proximal BCs (wired near the SAC soma) lag the distal BCs (wired far from the soma).

Such 'space–time wiring specificity' could lead to DS as follows (Fig. 1c). Motion outward from the soma will activate the proximal BCs followed by the distal BCs. If the stimulus speed is appropriate for the time lag, signals from both BC groups will reach the SAC dendrite simultaneously, summing to produce a large depolarization. For motion inward towards the soma, BC signals will reach the SAC dendrite asynchronously, causing only small depolarizations. Therefore the dendrite will 'prefer' outward motion, as observed experimentally[3].

Three-dimensional reconstruction by crowd and machine

We tested our hypothesis by reconstructing Off BC–SAC circuitry using e2198, an existing data set of mouse retinal images from serial block-face scanning electron microscopy (SBEM)[9]. The e2198 data set was oversegmented by an artificial intelligence into groups of neighbouring voxels that were subsets of individual neurons. These 'supervoxels' were assembled by humans into accurate three-dimensional (3D) reconstructions of neurons. For this activity, we hired and trained a small number of workers in the laboratory, and also transformed work into play by mobilizing volunteers through EyeWire, a website that turns 3D reconstruction of neurons into a game of colouring serial electron microscopy images.

Through EyeWire, we wanted to enable anyone, anywhere, to participate in our research. The approach is potentially scalable to extremely large numbers of 'citizen scientists'[10]. More importantly, the 3D reconstruction of neurons requires highly developed visuospatial abilities, and we wondered whether a game could be more effective[11] than traditional methods of recruiting and creating experts.

In gameplay mode, EyeWire shows a 2D slice through a 'cube', an e2198 subvolume of $256 \times 256 \times 256$ greyscale voxels (Fig. 2a). Gameplay consists of two activities: colouring the image near a location, or searching for a new location to colour. Colouring is done by clicking at any location in the 2D slice, which causes the supervoxel containing that location to turn blue. Searching is done by translating and orienting the slice within the cube, and interacting with a 3D rendering of the coloured supervoxels.

When the player first receives a cube, it already comes with a 'seed', a contiguous set of coloured supervoxels. The challenge is to colour all the rest of the supervoxels that belong to the same neuron, and avoid colouring other neurons. Gameplay for a cube terminates when the player clicks 'submit', receives a numerical score (Extended Data Fig. 1a), and proceeds to the next cube. Because our artificial intelligence is sufficiently accurate, colouring supervoxels is faster than manually colouring voxels, an older approach to 3D reconstruction[12].

[1]Brain & Cognitive Sciences Department, Massachusetts Institute of Technology, Cambridge, Massachusetts 02139, USA. [2]Electrical Engineering and Computer Science Department, Massachusetts Institute of Technology, Cambridge, Massachusetts 02139, USA. [3]Qualcomm Research, 5775 Morehouse Drive, San Diego, California 92121, USA. [4]Max-Planck Institute for Medical Research, D-69120 Heidelberg, Germany. [5]https://eyewire.org. †Present addresses: 601 N 42nd Street, Seattle, Washington 98103, USA (M.R.); Princeton Neuroscience Institute and Computer Science Deptartment, Princeton, New Jersey 08544, USA (H.S.S.); Gatsby Computational Neuroscience Unit, London WC1N 3AR, UK (S.C.T.).
*These authors contributed equally to this work.

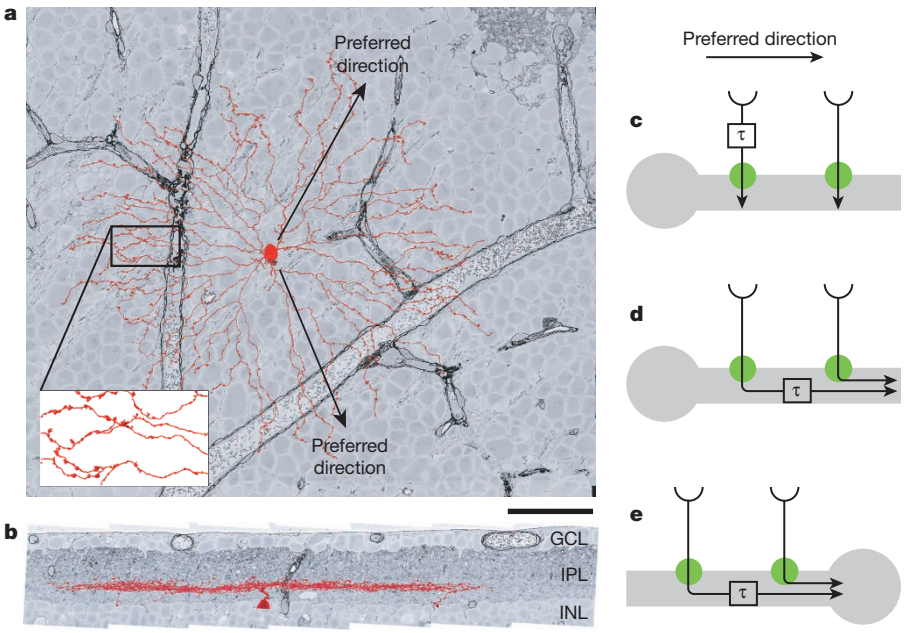

Figure 1 | Starburst amacrine cell and its direction selectivity. **a**, **b**, Off SAC (red) viewed opposite (**a**) and perpendicular (**b**) to the light axis. GCL, ganglion cell layer. Greyscale images from the e2198 data set[9]. Swellings of distal dendrites are presynaptic boutons (inset). Scale bar, 50 μm. **c**, We propose that a SAC dendrite is wired to pathways with time lags of visual response that differ by an amount τ. **d**, A previous model invoked the time lag due to signal conduction in a passive dendrite[24]. **e**, The previous model predicts an inward preferred direction for the somatic voltage, contrary to empirical observations[3].

The scoring system is designed to reward accurate colouring. This is nontrivial because EyeWire does not know the correct colouring. Each cube is assigned to multiple players (typically 5 to 10), and high scores are earned by players who colour supervoxels that other players also colour. In other words, the scoring system rewards agreement between players, which tends to be the same as rewarding accuracy.

Consensus is used not only to incentivize individual players, but also to enhance the accuracy of the entire system. Any player's colouring is equivalent to a set of supervoxels. Given the colourings of multiple players starting from the same seed in the same cube, a consensus can be computed by voting on each supervoxel. EyeWirer consensus was much more accurate than any individual EyeWirer (Fig. 2b, c).

Colouring a neuron is more challenging than it sounds. Images are corrupted by noise and other artefacts. Neurites take paths that are difficult to predict, and can branch without warning. Careless errors result from lapses in attention. Extensive practice is required to achieve accuracy. The most accurate EyeWirers (Fig. 2c, top right corner) often had experience with thousands of cubes. Improvements in accuracy were observed over the course of hundreds of cubes, corresponding to tens of hours of practice (Fig. 2d). According to subjective reports of EyeWirers, learning continues for much longer than that. By contrast, previous successes at 'crowdsourcing' image analysis involved tasks that did not require such extensive training[10,13].

Reconstructing an entire neuron requires tracing its branches through thousands of cubes. This process is coordinated by an automatic spawner, which inspects each consensus cube for branches that exit the cube. Each exit generates a new cube and seed, which are added to a queue. EyeWirers are automatically assigned to cubes by an algorithm that attempts to balance the number of plays for each cube.

Over 100,000 registered EyeWirers have been recruited by news reports, social media and the EyeWire blog. Players span a broad range of ages and educational levels, come from over 130 countries, and the

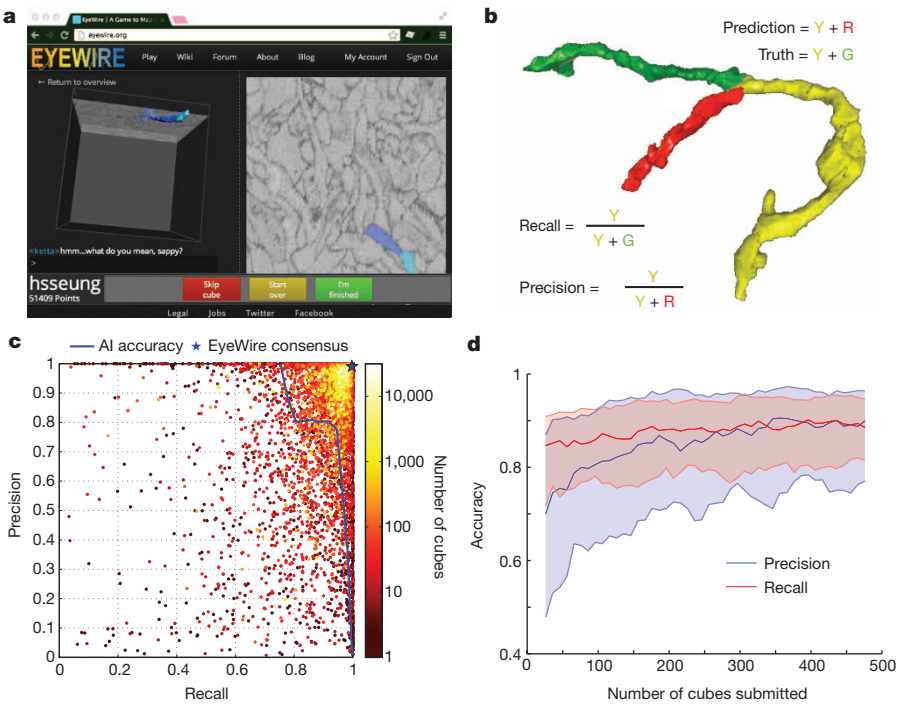

Figure 2 | EyeWire combines crowd and artificial intelligence. **a**, 3D and 2D views in the neuron reconstruction game. **b**, Precision and recall are two measures of accuracy. **c**, Accuracy of artificial intelligence (AI), 5,881 EyeWirers, and EyeWirer consensus on reconstruction of a ganglion cell. **d**, EyeWirer precision and recall increase with number of cubes submitted. Solid lines are median values across 208 EyeWirers who submitted at least 500 cubes, and shaded regions indicate 25th to 75th percentile.

great majority have no formal training in neuroscience (Extended Data Figs 2 and 3 and Supplementary Notes). These statistics show that EyeWire indeed widens participation in neuroscience research. At the same time, the most avid players constitute an elite group with disproportionate achievements. For example, the top 100 players have contributed about half of all cubes completed in EyeWire.

Laboratory workers also reconstructed neurons independently of EyeWire, with a more sophisticated version of the user interface (Methods). Their reconstructions were pooled with those of EyeWirers for the analyses reported below. Reconstruction error was quantified (Methods), and was treated like other kinds of experimental error when calculating confidence intervals from our data.

Contact analysis

We reconstructed 195 Off BC axons and 79 Off SACs from e2198 (Fig. 3b and Extended Data Fig. 4). The e2198 retina was stained in an unconventional way that did not mark intracellular structures such as neurotransmitter vesicles[9], and reliable morphological criteria for identification of BC presynaptic terminals are unknown. As an indirect measure of connectivity, contact areas were computed for all BC–SAC pairs. The resulting 'contact matrix' was analysed through two subsequent steps.

In the first step, Off BC axons were classified into five cell types, following structural criteria[14] established to correspond with previous molecular definitions[6] (Methods and Extended Data Fig. 5). BC types stratify at characteristic depths in the inner plexiform layer (IPL), and vary in size (Fig. 4a). The BCs of each type formed a 'mosaic', meaning that cells were spaced roughly periodically (Extended Data Fig. 6a–e). This is generally accepted as an important defining property of a retinal cell type. Type densities (Extended Data Fig. 6f) were roughly consistent with previous reports[6]. When the columns of the contact matrix were sorted by BC type (Fig. 4b), it became evident that BC2 and BC3a contact SACs more than other BC types.

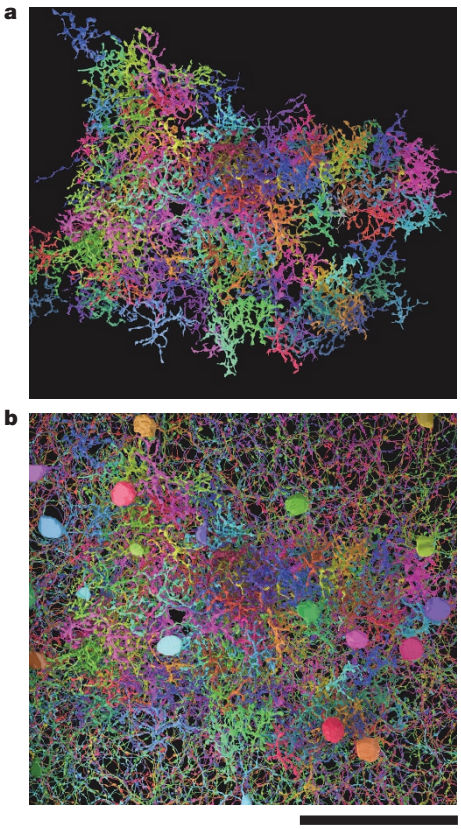

Figure 3 | 3D reconstructions of Off BCs and SACs. **a**, **b**, Cells viewed opposite the light axis. BCs alone (**a**); BCs with SACs (**b**). Scale bar, 50 µm.

In the second step, we averaged contact area over BC–SAC pairs of the same BC type and similar distance between the BC axon and the SAC soma in the plane tangential to the retina (Fig. 4c). These absolute areas were normalized to convert them into the percentage of SAC surface area covered by BCs of a given type (Methods). The resulting graphs show that BC2 prefers to contact SAC dendrites close to the SAC soma, whereas BC3a prefers to contact far from the soma (Fig. 4d and Extended Data Fig. 7c).

Imaging of intracellular calcium in BC axons[7] and extracellular glutamate around BC axons[8] indicates that BC2 lags BC3a in visual responses by 50–100 ms. Therefore BC–SAC wiring appears to possess the space–time specificity appropriate for an outward preferred direction, as we proposed (Fig. 1c).

Co-stratification analysis

Off SACs stratify at a particular depth in the IPL (Fig. 1b). Why this depth and not some other? From Fig. 4a, it is obvious that this depth is appropriate for wiring with BC2 and BC3a, as required by our model of DS emergence. Following this logic one step further, we wondered whether the observed dependence of contact on distance from the SAC soma might be reflected in fine aspects of SAC morphology. We hypothesized that SAC dendrites are 'tilted', moving deeper into the IPL with distance from the SAC soma. Such a change in depth would be compatible with more overlap with BC2 near the soma, and more overlap with BC3a far from the soma, as BC3a is deeper in the IPL than BC2 (Fig. 4a and Supplementary Video 1).

The hypothesized tilt turns out to exist (Fig. 5a). Very close to the SAC soma, the dendrites dive sharply into the IPL from the inner nuclear layer (INL). Surprisingly, IPL depth continues to increase as distance from the SAC soma in the tangential plane ranges from 20 to 80 µm. The slight increase is not evident in a single dendrite (Fig. 1b), but emerges from statistical averaging.

Could dendritic tilt be the cause of the observed variation in BC–SAC contact with distance (Fig. 4d)? We cannot address causality on the basis of our data, but we can test how well the tilt predicts contact variation. We computed the stratification profiles of BC types (Fig. 5a), defined as the one-dimensional density of BC surface area along the depth of the IPL. We also computed the stratification profile of SAC dendrites at various distances from the SAC soma (quartiles, Fig. 5a). Assuming that BC and SAC arborizations are statistically independent of each other, we estimated contact from 'co-stratification', defined as the integral over IPL depth of the product of BC and SAC stratification profiles (Methods).

We found that actual BC2 contact depends more strongly on distance than predicted; the slight change in IPL depth after the initial plunge appears too small to account for the large change in actual BC2 contact. In other failures of contact prediction, BC3a, BC3b and BC4 stratify at the same IPL depths (Fig. 5a), yet BC3a makes much more contact than BC3b or BC4. Also, actual BC3a contact plummets near the tips of SAC dendrites (Fig. 4d), whereas predicted contact does not change at all because the IPL depth of SAC dendrites is constant in this region (Fig. 5b). Overall, the total contact from all BC types seems low in this region (Extended Data Fig. 7d), suggesting that BCs avoid making synaptic inputs to the most distal SAC dendrites. This runs counter to the conventional belief that input synapses are uniformly distributed over the entire length of SAC dendrites[15]. The unreliability of inferring contact from co-stratification is illustrated by numerous examples of SAC dendrites that pass through BC axonal arborizations without making any contact at all (Extended Data Fig. 8).

Model of the BC–SAC circuit

We mentioned previously that BC2 lags BC3a in visual response. There is another important difference: BC3a responds more transiently to step changes in illumination, whereas BC2 exhibits more sustained responses. The implications of the sustained–transient distinction for DS can be understood using a mathematical model. The activity of a retinal neuron is often approximated as a linear spatiotemporal filtering of the visual

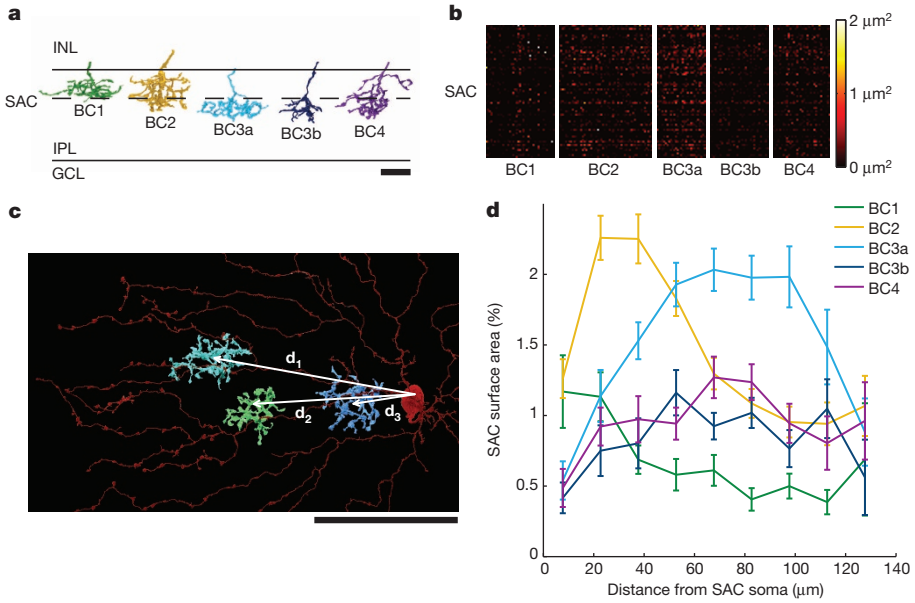

Figure 4 | BC–SAC contact. **a**, Off BCs were divided into five types[6,14] on the basis of IPL depth and size. Scale bar, 10 µm. **b**, Contact areas of BC–SAC pairs, sorted by BC types. **c**, Pairs were further sorted by the distance of the BC axon from the SAC soma, as measured in the tangential plane. Scale bar, 50 µm. **d**, Average BC–SAC contact versus distance, normalized to percentage of SAC surface area at that distance (Extended Data Fig. 3b). Standard error is based on the number of pairs for each BC type and distance (see Source Data for sample sizes).

stimulus followed by a nonlinearity[16,17]. Such a 'linear–nonlinear' model for the output $O(t)$ of the SAC dendrite can be written as

$$O(t) = \left[\int dx dt' \, W(x,t-t') I(x,t') \right]^{+} \quad (1)$$

For simplicity, the dendrite and visual stimulus $I(x,t)$ are restricted to a single spatial dimension x, and the nonlinearity is a half-wave rectification, $[z]^{+} = \max\{z,0\}$. We interpret the integral in equation (1) as the summed input from the BCs presynaptic to the SAC. The nonlinearity could arise from various biophysical mechanisms, such as synaptic transmission from SACs to other neurons. The spatiotemporal filter $W(x,t)$ is a sum of two functions,

$$W(x,t) = U_s(x) v_s(t) + U_t(x) v_t(t) \quad (2)$$

corresponding to contributions from BC2 and BC3a. The sustained temporal filter $v_s(t)$ is monophasic, whereas the transient filter $v_t(t)$ is biphasic (Fig. 6a). The spatial filter $U_s(x)$ represents the entire set of all BC2 inputs to the dendrite, and can be estimated from the BC2 contact area graph in Fig. 4d. Similarly, $U_t(x)$ can be estimated from the BC3a contact area graph. The two spatial filters are displaced relative to each other (Fig. 6a), because BC3a tends to contact SAC dendrites at more distal locations than BC2.

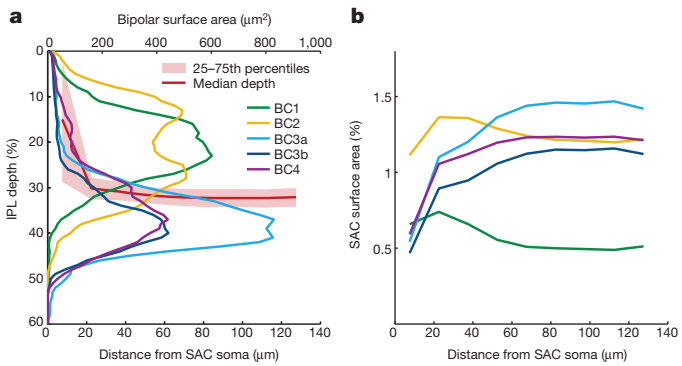

Figure 5 | BC–SAC co-stratification. **a**, SAC dendrites move deeper into the IPL (median depth, red line) with increasing distance from the SAC soma in the tangential plane. Stratification profiles of BC types, defined as density of surface area over the depth of the IPL. **b**, Co-stratification predictions of BC–SAC contact area versus distance from the SAC soma. The curves are normalized by SAC area at each distance, and are therefore directly comparable with those of Fig. 4d.

Each of the terms in the sum of equation (2) is said to be 'space–time separable', because it is the product of a function of space and a function of time. It was previously observed that a spatiotemporal filter $W(x,t)$ of this form can endow a model like equation (1) with DS[18,19]. This is illustrated by Fig. 6 using the fact that the convolution in equation (1) is equivalent to 'sliding' the spatiotemporal filter W in time over the stimulus I, and computing the overlap at each time. The filter $W(x,t)$ is oriented in space–time (Fig. 6a), and so also is a moving stimulus $I(x,t)$ (Fig. 6g, h). The overlap with a rightward-moving stimulus (Fig. 6h) is greater than for a leftward one (Fig. 6g), so the model exhibits DS with a rightward preferred direction.

How is DS affected by the biphasic shape of the transient temporal filter, $v_t(t)$? If we remove the negative lobe (Fig. 6c), then $v_t(t)$ will become monophasic like $v_s(t)$ and their relation closer to a simple time lag (Fig. 6d). We will refer to this model as a 'Reichardt detector', in honour of the pioneering researcher Werner Reichardt, although it more closely resembles a subunit of his model[20]. On the other hand, removing the positive lobe of $v_t(t)$ makes it monophasic but with inverted sign relative to the sustained filter (Fig. 6e). The result (Fig. 6f) resembles a DS model originally proposed by Barlow and Levick[21].

Both modified models (Fig. 6d, f) exhibit DS. In the Reichardt detector, the inputs from the two arms enhance each other for motion in the preferred direction. In the Barlow–Levick detector, the two inputs cancel each other for motion in the null direction. As our sustained–transient model (Fig. 6b) uses both mechanisms, it should exhibit more DS than either detector. Our model is related to versions of the Reichardt detector with low-pass and high-pass filters on the two arms[22].

In the original Barlow–Levick model, the negative filter corresponded to synaptic inhibition. As BCs are believed to be excitatory, negative BC input in our model represents a reduction of excitation relative to the resting level, rather than true inhibition. Signalling by reduced excitation may be possible, at least for low-contrast stimuli, as BC ribbon synapses may have a significant resting rate of transmitter release[23].

The model of equations (1) and (2) is a useful starting point for many theoretical investigations that are outside the scope of this article. For example, DS dependency on the spatial and temporal frequencies of a sinusoidal travelling wave stimulus is calculated in Supplementary Equations, and DS dependence on stimulus speed is graphed in Extended Data Fig. 9.

Discussion

In our DS model, SAC dendrites are wired to BC types with different time lags. A previous model did not distinguish between BC types, and instead relied on the time lag of signal conduction within the SAC dendrite itself[24]

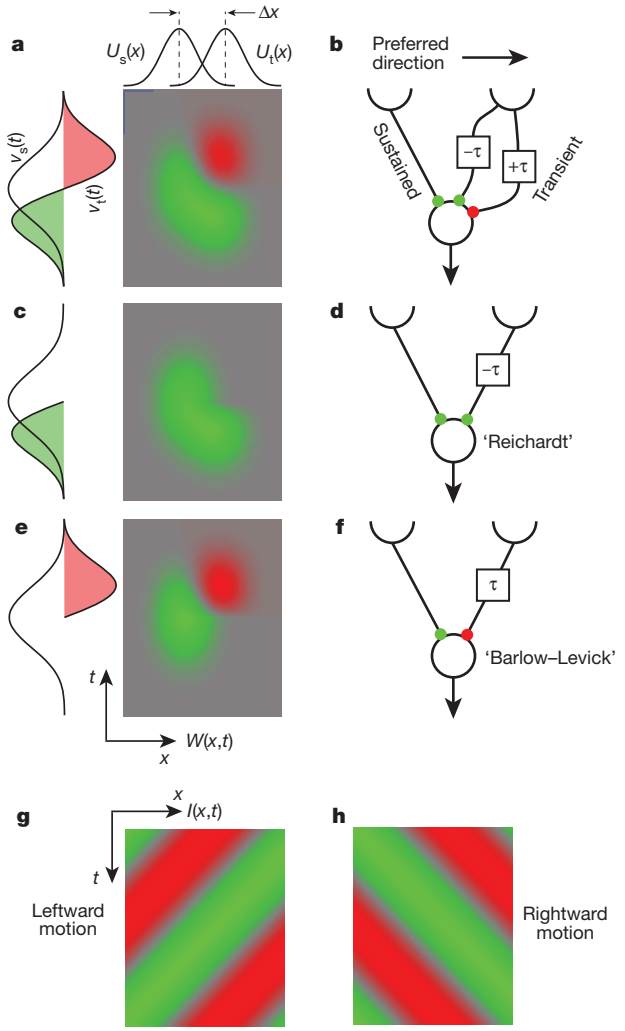

Figure 6 | Mathematical model of the BC–SAC circuit. **a**, Spatiotemporal filter of equation (2). Green is positive, red is negative, and grey is zero. **b**, The transient pathway effectively combines a positive channel that leads the sustained pathway by τ and a negative channel that lags by τ. **c**, Removing the negative channel yields a Reichardt detector (**d**). **e**, Removing the positive channel yields a Barlow–Levick detector (**f**). A moving visual stimulus $I(x,t)$ is oriented in space–time (**g**, **h**), and so are the spatiotemporal filters (**a**, **c**, **e**).

(Fig. 1d). Like most other amacrine cells, SACs lack an axon; their output synapses are found in the distal zones of their dendrites[15] (Fig. 1a, inset). Owing to dendritic conduction delay, proximal BC inputs should take longer to reach the output synapses than distal BC inputs (Fig. 1d). Therefore this time lag is also consistent with the empirical finding of an outward preferred direction. To summarize the novelty of our hypothesis, we place the time lag before BC–SAC synapses, whereas the previous model places it after BC–SAC synapses.

The postsynaptic delay model has a major weakness. If dendritic conduction were the only source of time lag, the somatic voltage would exhibit DS with an inward preferred direction, but this is inconsistent with intracellular recordings[3] (Fig. 1e). By contrast, the presynaptic delay model is compatible with approximating a SAC dendrite as isopotential (Fig. 1c), so preferred direction is predicted to be independent of the location of the voltage measurement, consistent with empirical data[3]. It may also be possible to make the postsynaptic delay model consistent with experiments by adding active dendritic conductances[4].

The presynaptic and postsynaptic delay models are not mutually exclusive. If they work together, passive cable theory suggests that presynaptic delay dominates, because estimated postsynaptic delay is much shorter than the time lag between BC2 and BC3a (Supplementary Equations). Can we gauge the relative importance of the delays empirically rather than theoretically? One way would be intracellular recording at the SAC soma of responses to visual stimulation at various dendritic locations. If postsynaptic delay dominates, then response latency will grow with distance of the visual stimulus from the soma. If presynaptic delay dominates, then distal stimulation will evoke somatic responses with shorter latency than proximal stimulation. This prediction may seem counterintuitive, but is an obvious outcome of our model.

Many other models of DS emergence in SACs invoke inhibition as well as excitation[25–28]. We have focused on excitatory mechanisms, as blocking inhibition does not abolish DS[3]. However, inhibition may have the effect of enhancing DS, and its role should be investigated further.

This work focused on Off BC–SAC circuitry. An analogous sustained–transient distinction can also be made for On BC types[7,8]. It remains to be seen whether their connectivity with On SACs depends on distance from the soma. If this turns out to be the case, then the model of Fig. 6 could serve as a general theory of motion detection by both On and Off SACs. The model filter of Fig. 6a also resembles the spatiotemporal receptive field of the J type of ganglion cell (see Fig. 3b of ref. 29).

Neural activity imaging[30] and connectomic analysis[31] have recently identified a plausible candidate for the site of DS emergence in the fly visual system. If our theory is correct, then the analogies between insect and mammalian motion detection[1] are more far-reaching than previously suspected, with fly T4 and T5 cells corresponding to On and Off SAC dendrites in both connectivity and function.

A glimmer of space–time wiring specificity can even be seen in the structure of the SAC itself. As BC types with different time lags arborize at different IPL depths, IPL depth can be regarded as a time axis. Therefore, the slight tilt of the SAC dendrites in the IPL (Fig. 5a) could be related to the orientation of the SAC receptive field in space–time (Fig. 6a). However, dendritic tilt alone is not sufficient to predict our model, as co-stratification sometimes fails to predict contact (Figs 4d and 5b). For example, co-stratification predicts strong BC4 connectivity to distal SAC dendrites. This would favour an inward preferred direction, contrary to what is observed, because BC2 leads (not lags) BC4 in visual responses[7].

The idea that contact (or connectivity) can be inferred from co-stratification is sometimes known as Peters' rule[32], and has also been applied to estimate neocortical connectivity[33–35]. The present work shows that fairly subtle violations of Peters' rule may be important for visual function. Previous research suggests that On–Off direction-selective ganglion cells inherit their DS from SAC inputs owing to a strong violation of Peters' rule[9,36–38].

Our findings were made possible by using artificial intelligence to reduce the amount of human effort required for 3D reconstruction of neurons. Even after the labour savings, our research required great human effort from a handful of paid workers in the laboratory and a large number of volunteers through EyeWire. Our experiences do not support claims that the 'wisdom of the crowd' should replace experts[39]. Instead, EyeWire depends on cooperation between laboratory experts and online amateurs (Methods). Furthermore, some amateurs developed remarkable expertise and were promoted to increasingly sophisticated roles within the EyeWire community (Supplementary Notes). We believe that crowd wisdom requires amplifying the expert voices within the crowd, and also empowering individuals to become experts. Fortunately, such goals are well-matched to the game format.

The EyeWire artificial intelligence was based on a deep convolutional network[40,41]. Similar networks have been successfully applied to serial electron microscopy images obtained using conventional staining techniques that mark intracellular organelles[42]. Extending EyeWire to such images, in which synapses are clearly visible, would enable a true connection analysis that goes beyond the contact and co-stratification analyses used here.

Our work demonstrates that reconstructing a neural circuit can provide surprising insights into its function. Much more will be learned as reconstruction speed grows. The combination of crowd and artificial intelligence promises a continuous upward path of improvement, as human input from the crowd is not only useful for generating neuroscience

discoveries, but also for making the artificial intelligence more capable through machine learning.

Note added in proof: Further evidence that BC axons exhibit little or no DS appeared while this paper was in press[43].

METHODS SUMMARY

A convolutional network was trained to detect neural boundaries via the MALIS procedure[40] and CNPKG (https://github.com/sriniturага/cnpkg/), which is based on Cortical Network Simulator[44]. The convolutional network was applied to the e2198 data set, which was then segmented into supervoxels by a modified version of the watershed algorithm. Paid workers and volunteer EyeWirers reconstructed neurons in 3D by assembling supervoxels. The retina was computationally flattened, reconstructed neurons were classified by their structural properties, and contact and co-stratification were analysed by custom Matlab and C++ code.

Online Content Any additional Methods, Extended Data display items and Source Data are available in the online version of the paper; references unique to these sections appear only in the online paper.

Received 13 October 2013; accepted 10 March 2014.
Published online 4 May 2014.

1. Borst, A. & Euler, T. Seeing things in motion: models, circuits, and mechanisms. *Neuron* **71,** 974–994 (2011).
2. Vaney, D. I., Sivyer, B. & Taylor, W. R. Direction selectivity in the retina: symmetry and asymmetry in structure and function. *Nature Rev. Neurosci.* **13,** 194–208 (2012).
3. Euler, T., Detwiler, P. B. & Denk, W. Directionally selective calcium signals in dendrites of starburst amacrine cells. *Nature* **418,** 845–852 (2002).
4. Hausselt, S. E., Euler, T., Detwiler, P. B. & Denk, W. A dendrite-autonomous mechanism for direction selectivity in retinal starburst amacrine cells. *PLoS Biol.* **5,** e185 (2007).
5. Yonehara, K. *et al.* The first stage of cardinal direction selectivity is localized to the dendrites of retinal ganglion cells. *Neuron* **79,** 1078–1085 (2013).
6. Wässle, H., Puller, C., Müller, F. & Haverkamp, S. Cone contacts, mosaics, and territories of bipolar cells in the mouse retina. *J. Neurosci.* **29,** 106–117 (2009).
7. Baden, T., Berens, P., Bethge, M. & Euler, T. Spikes in mammalian bipolar cells support temporal layering of the inner retina. *Curr. Biol.* **23,** 48–52 (2013).
8. Borghuis, B. G., Marvin, J. S., Looger, L. L. & Demb, J. B. Two-photon imaging of nonlinear glutamate release dynamics at bipolar cell synapses in the mouse retina. *J. Neurosci.* **33,** 10972–10985 (2013).
9. Briggman, K. L., Helmstaedter, M. & Denk, W. Wiring specificity in the direction-selectivity circuit of the retina. *Nature* **471,** 183–188 (2011).
10. Lintott, C. J. *et al.* Galaxy Zoo: morphologies derived from visual inspection of galaxies from the Sloan Digital Sky Survey. *Mon. Not. R. Astron. Soc.* **389,** 1179–1189 (2008).
11. Cooper, S. *et al.* Predicting protein structures with a multiplayer online game. *Nature* **466,** 756–760 (2010).
12. Fiala, J. C. Reconstruct: a free editor for serial section microscopy. *J. Microsc.* **218,** 52–61 (2005).
13. Von Ahn, L. & Dabbish, L. Labeling images with a computer game. In *Proceedings of the SIGCHI Conference on Human Factors in Computing Systems* 319–326 (ACM, 2004).
14. Helmstaedter, M. *et al.* Connectomic reconstruction of the inner plexiform layer in the mouse retina. *Nature* **500,** 168–174 (2013).
15. Famiglietti, E. V. Synaptic organization of starburst amacrine cells in rabbit retina: analysis of serial thin sections by electron microscopy and graphic reconstruction. *J. Comp. Neurol.* **309,** 40–70 (1991).
16. Berry, M. J., II & Meister, M. Refractoriness and neural precision. *J. Neurosci.* **18,** 2200–2211 (1998).
17. Baccus, S. A. & Meister, M. Fast and slow contrast adaptation in retinal circuitry. *Neuron* **36,** 909–919 (2002).
18. Watson, A. B. & Ahumada, A. J. Jr. Model of human visual-motion sensing. *J. Opt. Soc. Am. A* **2,** 322–341 (1985).
19. Adelson, E. H. & Bergen, J. R. Spatiotemporal energy models for the perception of motion. *J. Opt. Soc. Am. A* **2,** 284–299 (1985).
20. Reichardt, W. in *Sensory Communication* (ed. Rosenblith, W. A.) 303–317 (MIT Press, 1961).
21. Barlow, H. B. & Levick, W. R. The mechanism of directionally selective units in rabbit's retina. *J. Physiol. (Lond.)* **178,** 477–504 (1965).
22. Borst, A., Reisenman, C. & Haag, J. Adaptation of response transients in fly motion vision. II: model studies. *Vision Res.* **43,** 1311–1324 (2003).
23. Lagnado, L., Gomis, A. & Job, C. Continuous vesicle cycling in the synaptic terminal of retinal bipolar cells. *Neuron* **17,** 957–967 (1996).
24. Tukker, J. J., Taylor, W. R. & Smith, R. G. Direction selectivity in a model of the starburst amacrine cell. *Vis. Neurosci.* **21,** 611–625 (2004).
25. Borg-Graham, L. J. & Grzywacz, N. M. in *Single Neuron Computation* (eds McKenna, T., Davis, J. & Zornetzer, S. F.) Ch. 13, 347–76 (Academic San Diego, 1992).
26. Gavrikov, K. E., Dmitriev, A. V., Keyser, K. T. & Mangel, S. C. Cation–chloride cotransporters mediate neural computation in the retina. *Proc. Natl Acad. Sci. USA* **100,** 16047–16052 (2003).
27. Münch, T. A. & Werblin, F. S. Symmetric interactions within a homogeneous starburst cell network can lead to robust asymmetries in dendrites of starburst amacrine cells. *J. Neurophysiol.* **96,** 471–477 (2006).
28. Lee, S. & Zhou, Z. J. The synaptic mechanism of direction selectivity in distal processes of starburst amacrine cells. *Neuron* **51,** 787–799 (2006).
29. Kim, I.-J., Zhang, Y., Yamagata, M., Meister, M. & Sanes, J. R. Molecular identification of a retinal cell type that responds to upward motion. *Nature* **452,** 478–482 (2008).
30. Maisak, M. S. *et al.* A directional tuning map of *Drosophila* elementary motion detectors. *Nature* **500,** 212–216 (2013).
31. Takemura, S. Y. *et al.* A visual motion detection circuit suggested by *Drosophila* connectomics. *Nature* **500,** 175–181 (2013).
32. Braitenberg, V. & Schüz, A. *Cortex: Statistics and Geometry of Neuronal Connectivity* 2nd edn (Springer Berlin, 1998).
33. Kalisman, N., Silberberg, G. & Markram, H. Deriving physical connectivity from neuronal morphology. *Biol. Cybern.* **88,** 210–218 (2003).
34. Binzegger, T., Douglas, R. J. & Martin, K. A. C. A quantitative map of the circuit of cat primary visual cortex. *J. Neurosci.* **24,** 8441–8453 (2004).
35. Stepanyants, A. & Chklovskii, D. B. Neurogeometry and potential synaptic connectivity. *Trends Neurosci.* **28,** 387–394 (2005).
36. Fried, S. I., Münch, T. A. & Werblin, F. S. Mechanisms and circuitry underlying directional selectivity in the retina. *Nature* **420,** 411–414 (2002).
37. Yonehara, K. *et al.* Spatially asymmetric reorganization of inhibition establishes a motion-sensitive circuit. *Nature* **469,** 407–410 (2010).
38. Wei, W., Hamby, A. M., Zhou, K. & Feller, M. B. Development of asymmetric inhibition underlying direction selectivity in the retina. *Nature* **469,** 402–406 (2011).
39. Surowiecki, J. *The Wisdom of Crowds* (Anchor, 2005).
40. Turaga, S., Briggman, K., Helmstaedter, M., Denk, W. & Seung, H. S. in *Advances in Neural Information Processing Systems 22*, 1865–1873 (2009).
41. Turaga, S. C. *et al.* Convolutional networks can learn to generate affinity graphs for image segmentation. *Neural Comput.* **22,** 511–538 (2010).
42. Ciresan, D. *et al.* in *Advances in Neural Information Processing Systems 25*, 2852–2860 (2012).
43. Park, S. J. H., Kim, I.-J., Looger, L. L., Demb, J. B. & Borghuis, B. G. Excitatory synaptic inputs to mouse on-off direction-selective retinal ganglion cells lack direction tuning. *J. Neurosci.* **34,** 3976–3981 (2014).
44. Mutch, J., Knoblich, U. & Poggio, T. *CNS: a GPU-Based Framework for Simulating Cortically-Organized Networks* Tech. Rep. MIT-CSAIL-TR-2010–013/CBCL-286 (MIT, 2010).

Supplementary Information is available in the online version of the paper.

Acknowledgements This research was made possible by funding from the Gatsby Charitable Foundation, the Howard Hughes Medical Institute, the Human Frontier Science Program, an anonymous donor, and the National Institutes of Health. K.L. was supported by a Samsung Scholarship. Support from the AWS Research Grants Program gave EyeWire global reach through Amazon Cloudfront. We thank K. Briggman for providing the e2198 data set. J. Mutch created the CNS framework on which CNPKG is based. D. Jia, R. Shearer, and B. Warne assisted in early stages of software development, and W. Silversmith with recent modifications. R. Prentki, L. Trawinski, M. Sorek, A. Ostojic, C. David, R. Avery, S. Temple, A. Bost, M. Greenstein and M. Evans worked in the laboratory to reconstruct neurons, and the first six also served as GrimReaper and hosted EyeWire competitions. Additional reconstructions were provided by R. Han, M. Gavrin, G. Lu, A. Ortiz and D. Udvary. All were trained by R. Prentki, who also created training videos for EyeWirers. We are grateful to A. Norton for 3D renderings, and to E. Almeida for EyeWire graphics. We acknowledge discussions with T. Baden, M. Berry, B. Borghuis, A. Borst, E. J. Chichilnisky, D. Chklovskii, D. Clark, J. Demb, T. Euler, M. Helmstaedter, A. Huberman, S. Lee, R. Masland, J. Sanes and Z. Zhou.

Author Contributions J.S.K. created algorithms, software and procedures for crowd intelligence and learning, and applied them to generate neuron reconstructions. J.S.K. and M.J.G. classified bipolar cells. M.J.G. analysed contact and co-stratification, aided by code from A.Z. and input from W.D. H.S.S. devised the model with help from B.F.B. and M.C. S.C.T. trained the convolutional network. M.P. and M.B. implemented software and algorithms created by A.Z. for interactive segmentation and 3D visualization, with guidance from S.C.T. M.R. created the EyeWire game and M.B. its data infrastructure. K.L. quantified EyeWirer accuracy and learning. A.R. mobilized and studied the EyeWire community. EyeWirers reconstructed neurons and built extensions to EyeWire. H.S.S. wrote the paper with help from J.S.K., M.J.G. and A.R.

Author Information Reprints and permissions information is available at www.nature.com/reprints. The authors declare competing financial interests: details are available in the online version of the paper. Readers are welcome to comment on the online version of the paper. Correspondence and requests for materials should be addressed to H.S.S. (sseung@princeton.edu).